Synoptic Pattern and Severe Weather Associated with the Wide Convection over Southeast China During the Summer Monsoon Period

WANG Hui[1,2] (汪 会), LUO Yali[1,3*] (罗亚丽), and ZHANG Renhe[1] (张人禾)

1 *State Key Laboratory of Severe Weather, Chinese Academy of Meteorological Sciences, Beijing* 100081

2 *Key Laboratory for Cloud Physics and Weather Modification of China Meteorological Administration, Chinese Academy of Meteorological Sciences, Beijing* 100081

3 *Collaborative Innovation Center on Forecast and Evaluation of Meteorological Disasters, Nanjing University of Information Science & Technology, Nanjing* 210044

(Received May 23, 2014; in final form July 29, 2014)

ABSTRACT

Based on the Tropical Rainfall Measuring Mission (TRMM) precipitation radar observations, wide convection (WC) is defined as contiguous convective echoes over 40 dBZ, accompanied with a near surface rainfall area exceeding 1000 km^2. In Southeast China, the maximal occurrence frequency of WC takes place over the flat land region in the central plain of East China during the summer monsoon period of 1998–2010. When WC occurs in this region, the 500-hPa atmospheric fields are categorized into three patterns by using an objective classification method, i.e., the deep-trough-control (DTr) pattern, the subtropical-high-maintenance (STH) pattern, and the typhoon-effect (Typh) pattern, which respectively accounts for 20.8%, 52.8%, and 26.4% of the total WC occurrences. The DTr pattern starts to emerge the earliest (16–31 May) and occurs the most often in the second half of June; the STH pattern has a significant occurrence peak in the first half of July; the Typh pattern occurs mostly in July and August.

Nearly all WC occurrences in this region are associated with thunderstorms, due to large convective available potential energy and abundant moisture. Among the three synoptic patterns, the DTr pattern features the driest and coldest air in the region, leading to the least occurrences of short-duration heavy rainfall. Strong winds occur the most often under the DTr pattern, probably owing to the largest difference in air humidity between the mid and low troposphere. Hail at the surface is rare for all occurrences of WC, which is probably related to the humid environmental air under all weather patterns and the high (> 5 km) freezing level under the STH pattern.

Key words: Tropical Rainfall Measuring Mission (TRMM), wide convection, central plain of East China, synoptic condition, severe weather

Citation: Wang Hui, Luo Yali, and Zhang Renhe, 2015: Synoptic pattern and severe weather associated with the wide convection over Southeast China during the summer monsoon period. *J. Meteor. Res.*, **29**(1), 041–058, doi: 10.1007/s13351-014-4069-4.

1. Introduction

Precipitation over China is closely related to the summer monsoon activities (Ding and Chan, 2005). Occurrence frequency and intensity of heavy rainfall over East China increase significantly after the onset of the South China Sea (SCS) monsoon in May, while the first rainy season over the mainland of China starts in April (Wang et al., 2004; Ding and Wang, 2008). Influence of the summer monsoon on precipitation over China generally lasts until the end of August (Ding, 1994). During the summer monsoon period, floods occur frequently and cause serious economic losses and quantities of casualties in East China (Huang et al., 2004). More than 90% of the monsoon rainfall in East China is contributed by precipitation systems that

Supported by the National (Key) Basic Research and Development (973) Program of China (2012CB417202), National Natural Science Foundation of China (41175049 and 41221064), National Science and Technology Support Program of China (2012BAC22B03), and Basic Research Fund of the Chinese Academy of Meteorological Sciences (2012Y001).

*Corresponding author: yali@cams.cma.gov.cn.

present convective features (Luo et al., 2013).

Convective intensity of storms is of importance because of its close association with the rainfall intensity, wind speed, and hail amount at the surface, and thus societal and economic impacts. Vertical velocity of air mass in a storm is probably the most accurate and direct parameter to measure the convective intensity of storms; but observation of air vertical velocity is lacking around the world. While the launch of the Tropical Rainfall Measuring Mission (TRMM; Kummerow et al., 2001) aims at detecting three-dimensional (3D) structures of precipitation systems, many studies have applied the TRMM data as a measurement or estimation of convective intensity of precipitating systems. The commonly used parameters based on the TRMM observations include the vertical profile of maximum reflectivity, minimum polarization corrected temperatures at 85 and 37 GHz, and flash rate (Cecil et al., 2002, 2005; Zipser et al., 2006). The 3D echo structures viewed by TRMM precipitation radar (PR; Kawanishi et al., 2000) have also been used to classify precipitation systems, especially those in association with extreme echo structures. For example, Houze et al. (2007) and Romatschke et al. (2010) identified three extreme echo structures: deep convective cores, wide convective cores, and broad stratiform regions (Fig. 3 in Romatschke et al., 2010, showing examples of the extreme echo structures), and investigated the temporal and spatial variations of the extreme convection in South Asia.

As the precipitation of East China is highly convective, knowledge of the convective structure and processes over this region is helpful for understanding climatological patterns of rain in the region. Wide convection (WC), defined as contiguous convective echoes over 40 dBZ with nonzero near surface rainfall rate from PR (Iguchi et al., 2000) over a horizontal area exceeding 1000 km^2, is often located within mature mesoscale convective systems (MCSs) with a large convective area and probably in association with severe convective weather. However, study on the statistics of WC in China has not been done so far. This study investigates the WC viewed by TRMM PR over Southeast China and its vicinity (land region of 15°–35°N, 105°–125°E; Fig. 1b) where the largest amount of precipitation occurs during the Asian summer monsoon period.

There are a total of 697 WC occurrences over Southeast China and its vicinity during the period from the SCS monsoon onset to the end of August during 1998–2010. The WC occurrences are extreme in the sense that they account for only 0.19% of the TRMM PR observed rainy storm population. Their distribution (Fig. 1b) clearly suggests that the WC tends to occur the most often over the flat land region of central East China (i.e., 31°–35°N, 114°–121°E), herein referred to as the central plain of East China or the control region. This region is highly populated, contributing a significant share of economy of China. Classification of synoptic weather patterns for the WC and understanding of the associated severe weather phenomena are helpful for severe weather forecasting in this region and therefore of practical importance.

The WC over the central plain of East China is the focus of this study. The main objectives are: (1) to identify major synoptic weather patterns for the WC occurrences and their subseasonal variations; (2) to investigate occurrences of severe convective weather phenomena in association with the WC; and (3) to quantify the corresponding environmental atmospheric conditions that are relevant to development of distinctive convective weather phenomena. This paper is organized as follows. Section 2 describes the data and methodology. Section 3 describes classification of synoptic patterns, and Section 4 presents subseasonal variations of the WC. Section 5 provides the statistics of severe convective weather phenomena corresponding to each of the identified synoptic patterns. The corresponding environmental atmospheric conditions are introduced in Section 6. Section 7 gives the summary and discussion of this article.

2. Data and methodology

2.1 TRMM data

In this study, the University of Utah TRMM Level-1 database is used to identify WC and to anal-

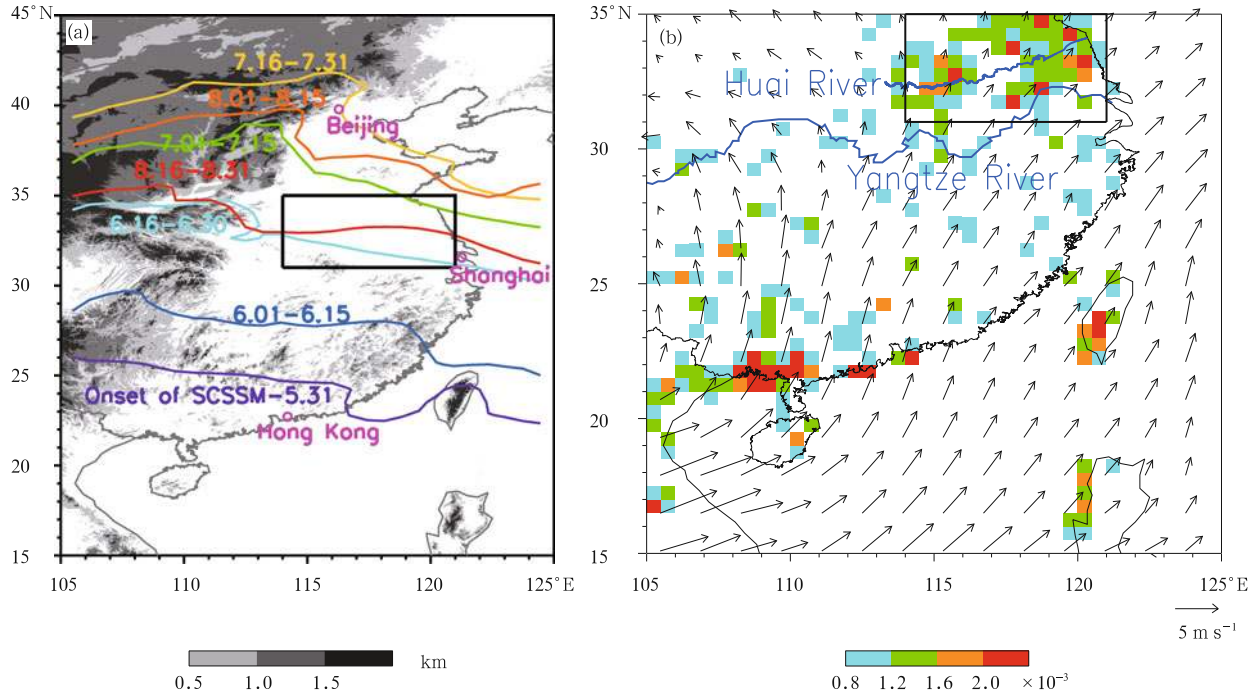

Fig. 1. (a) Topography map overlaid by the average θ_e = 345 K isolines at 850 hPa in East China and its vicinity from the onset of SCS summer monsoon (SCSSM) to 31 May, and each half month of 1–15 June, 16–30 June, 1–15 July, 16–31 July, 1–15 August, and 16–31 August. These isolines are the mean for 1998–2010. The cities of Beijing, Shanghai, and Hong Kong (pink circles) are labeled. (b) Geographical distribution of occurrence frequency of the WC in Southeast China and its vicinity (shadings), which is calculated as number of pixels of WC divided by the total number of TRMM pixels for each 0.5° × 0.5° grid. The horizontal winds at 850 hPa averaged form the onset of SCSSM to the end of August of 1998–2010 (black arrows) are based on the ERA-interim data. The Yangtze and Huai rivers are marked with blue lines. The black rectangle in each panel represents location of the central plain of East China.

yze the geographical distribution of WC occurrences. The dataset is developed by Liu et al. (2008), produced by collocation of measurements from four different instruments aboard the TRMM satellite: PR, TRMM Microwave Imager, Visible and Infrared Scanner, and Lightning Imaging Sensor (Liu, 2007). Information of 3D distribution of radar reflectivity of cloud and precipitation at the coordinates of PR pixels is used in the present study.

2.2 ERA-interim data

The ERA-interim (Simmons et al., 2007; Dee et al., 2011) reanalysis data from the ECMWF provide atmospheric variables four times per day (at 0000, 0600, 1200, and 1800 UTC). They are analyzed herein to reveal the synoptic weather patterns and the environmental thermodynamic conditions related to development of the WC.

2.3 Surface observations

Quality-controlled surface observations at global meteorological stations from 1998 to 2010 are obtained from the National Meteorological Information Center (NMIC) of China Meteorological Administration (CMA) (http://mdss.cma.gov.cn:8080/shuju/index3.jsp?tpcat=SURF&dsid=SURF_WEA_GLB_MUL_FTM_QC&type=file). The observations are available four times (0000, 0600, 1200, and 1800 UTC) per day. There are 56 surface observation stations quite evenly distributed in the central plain of East China. The elements extracted from this dataset include observation date/time, longitude and latitude of station, wind speed, 6-h accumulated rainfall, and weather phenomenon.

Four kinds of severe convective weather phenomena are analyzed in this study, including thunderstorm, gale, hail, and short-duration heavy rainfall.

Thunderstorm and hail are determined by directly referring to the observation of weather phenomenon in the surface observation dataset; gale is defined as the wind speed at the station turns greater than 17 m s^{-1}; short-duration heavy rainfall is considered as the accumulated rainfall during the past 6 h (R_{6h}) is larger than 20, 30, or 50 mm, respectively. Occurrence of a severe convective weather phenomenon at a certain time in the central plain of East China is defined as this severe convective weather phenomenon was observed over at least 1 of the 56 surface stations in the region during 1998–2010.

2.4 Definition of WC

The definition of WC is similar to the definition of "wide convective cores" by Houze et al. (2007) and Romatschke et al. (2010), who defined wide convective cores as contiguous convective echoes of $\geqslant$ 40 dBZ over a horizontal area of $\geqslant$ 1000 km^2. With such extensive intense convective cores, the WC often occurs within extremely broad MCSs with large convective areas. Compared to precipitation systems that are the most intense as measured by proxies at the PR pixel-level (e.g., maximum reflectivity at 6-km altitude, maximum height of the 40-dBZ echo), this type of precipitation system generally has larger horizontal span and larger near surface volumetric rainfall. As examples, Fig. 2 shows properties of three WCs observed by TRMM on 17 May 2008, 29 June 2006, and 20 July 2003, respectively. Clearly, the convective cores were embedded inside a large rainy area where the radar echo was weak and generally smoothly distributed. The convective area was 11233, 16463, and 6838 km^2, respectively, accounting for about 28%, 35%, and 21% of each MCS's total area. The volumetric rainfall of the MCS was 179827, 258677, and 74080 mm h^{-1} km^2, respectively, with 68%, 70%, and 54% contribution from convective rain. A majority of the convective cores had tops located between 6- and 9-km altitudes, although they could occasionally reach up to 12 km.

2.5 Definition of the onset date of the SCS summer monsoon

The onset date of the SCS summer monsoon is defined following the criterion of CMA National Climate Center (http://cmd.ncc.cma.gov.cn/Monitoring/monsoon.htm), which is the day when horizontal zonal wind at 850 hPa stably changes from easterly to westerly and the pseudo-equivalent potential temperature (θ_e) at 850 hPa becomes larger than 340 K over 10°–20°N, 110°–120°E. The onset dates of the SCS summer monsoon during 1998–2010 are given in Table 1.

Table 1. Onset dates of the SCS summer monsoon during 1998–2010

Year	Onset date of the SCS summer monsoon
1998	May 19
1999	May 23
2000	May 11
2001	May 07
2002	May 13
2003	May 22
2004	May 19
2005	May 26
2006	May 17
2007	May 21
2008	May 05
2009	May 26
2010	May 22

3. Classification and characteristics of synoptic patterns

There are 212 WC occurrences detected by TRMM over the central plain of East China from the onset of the SCS summer monsoon to the end of August during 1998–2010. According to the 500-hPa geopotential height pattern over East Asia (15°–45°N, 100°–130°E) during the period when WC was detected by TRMM, three synoptic weather patterns of the WC were identified by using a two-step method as follows.

(1) Possible impact of a typhoon was considered firstly. If the center of a typhoon was located less than 1500 km from the boundary of the control region, the typhoon may have some effect on the WC. The corresponding synoptic pattern was categorized as the typhoon-effect (Typh) type.

(2) KMEANS clustering (Anderberg, 1973) was

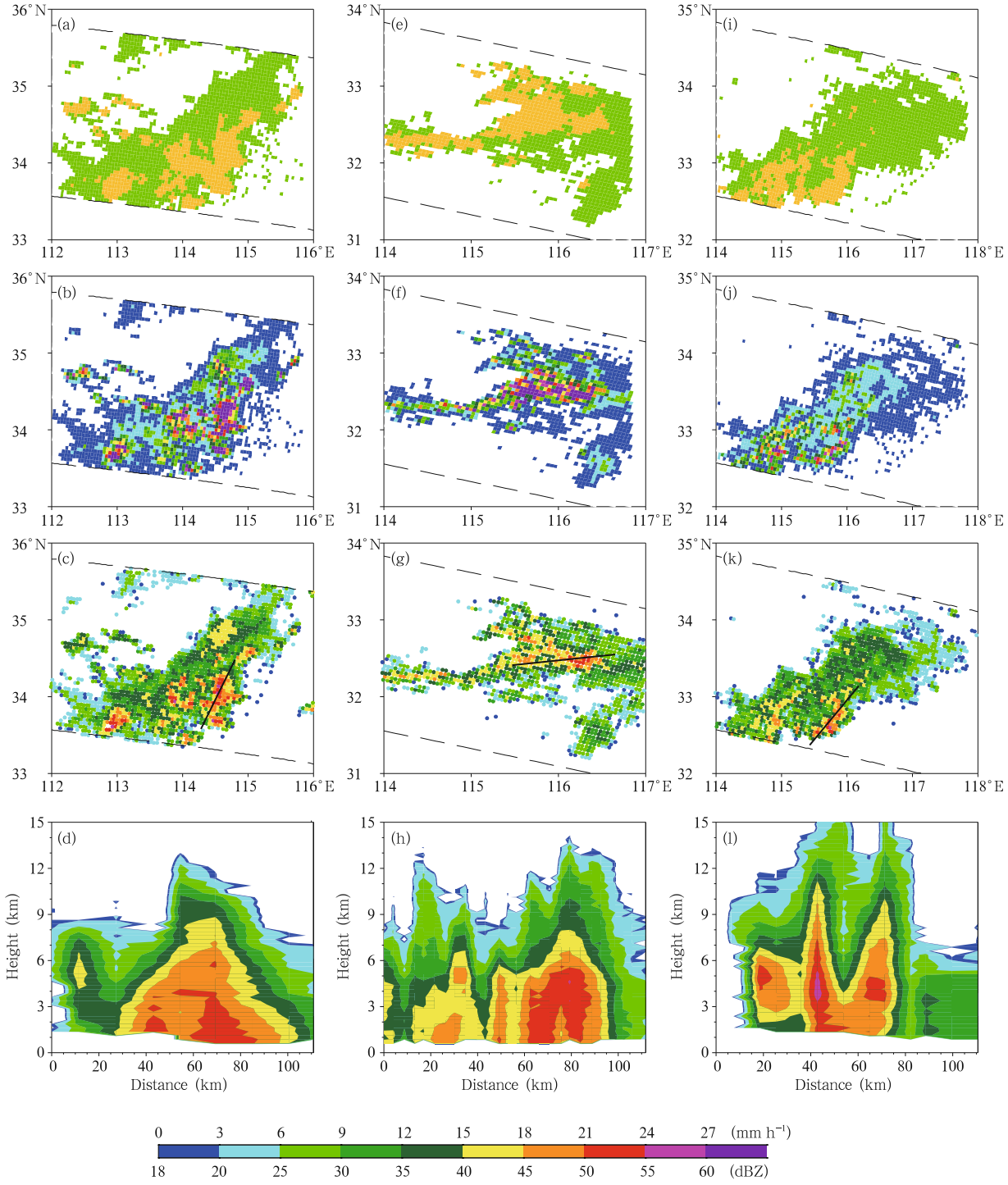

Fig. 2. Three examples of TRMM PR fields that exhibited the wide convection at (a–d) 1232 UTC 17 May 2008, (e–h) 0208 UTC 29 June 2006, and (i–l) 1805 UTC 20 July 2003. The first row shows rain types from the TRMM 2A23 algorithm (Awaka et al., 1998) where yellow and green indicate convective and stratiform rainfall, respectively; the second and third rows respectively show the horizontal cross-sections of near surface rain rate derived from the TRMM PR (Iguchi et al., 2000) and radar reflectivity at 3-km altitude; the last row shows vertical cross-sections of radar reflectivity through the black solid lines in the third row. The black dashed lines in the upper three rows represent the boundaries of the TRMM PR scan.

applied to classification of synoptic weather patterns for the other WC cases. A predefined number of clusters, being 2 and 3, respectively, was tested, and distributions of the clustering centers are shown in Fig. 3. The key results of the analysis are the mean pattern within each cluster and the number of cases within each cluster. With the number of clusters being 2, two distinctive synoptic weather patterns were obtained: a deep trough controls the central plain of East China ($C2_1$; Fig. 3a), and a northwestern Pacific subtropical high maintains around the south of the control region interacting with a trough to the north ($C2_2$; Fig. 3b). When the clustering number was increased to 3 (Figs. 3c–e), the first pattern ($C3_1$) was very similar to $C2_1$ and the other two patterns ($C3_2$ and $C3_3$) resemble $C2_2$, i.e., they were both characterized with the northwestern Pacific subtropical high interacting with a trough to the north, but the northwestern Pacific subtropical high was located more southward in $C3_2$ and more northward in $C3_3$ compared to $C2_2$. In order to ensure uniqueness of the classified synoptic weather patterns, the results with the number of clusters being 2 are adopted. The classified synoptic weather patterns ($C2_1$ and $C2_2$) are named the deep-trough-control (DTr) pattern and the subtropical-high-maintenance (STH) pattern, respectively.

Therefore, the synoptic weather patterns of the WC are categorized into three types, namely, DTr, STH, and Typh. Some examples are given in Figs. 4–6. The major characteristics of the three synoptic weather patterns are described below and summarized in Table 2.

The DTr pattern is characterized with a quasi-south-north oriented deep trough extending southward to about 30°N, controlling the central plain of East China. More than half (68%) of the deep troughs extended from a cold vortex, i.e., a cold core cyclonic center at 500 hPa (e.g., Fig. 4c). There were 44 WC cases detected under this synoptic weather pattern, accounting for 20.8% of the total WC cases. Among the WC cases under the DTr pattern, 50% occurred pre (i.e., east of) the deep trough (Figs. 4a and 4c), and the other 50% occurred post (i.e., west of) the deep trough (Fig. 4b). Under the DTr pattern, the central plain of East China was usually influenced by cold air invading as suggested by the cold thermal advection at 500 hPa (e.g., Figs. 4a–c).

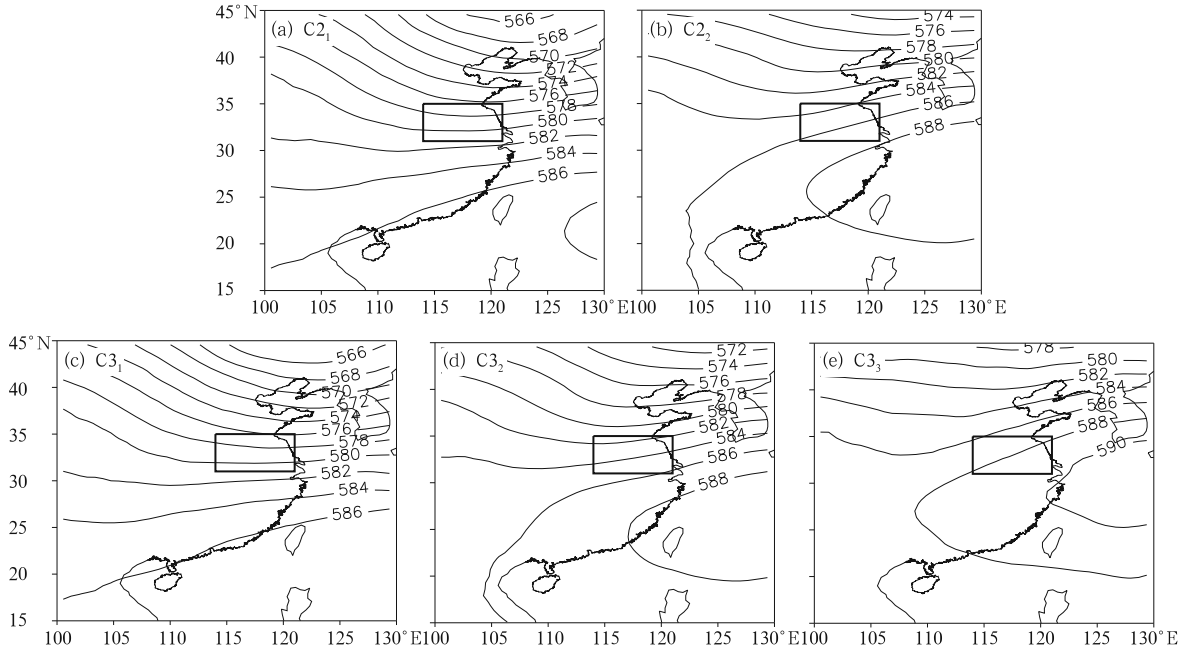

Fig. 3. The clustering centers based on KMEANS clustering for 500-hPa geopotential height over East Asia (15°–45°N, 100°–130°E) with the clustering number of (a, b) 2 and (c–e) 3, respectively.

Table 2. Summary of the attributes of the synoptic weather patterns (DTr, STH, and Typh) for the WC cases in the central plain of East China: characteristics at 500 hPa, number and fraction (%) of the WC, number of proximal ERA-interim dates of the WC, and location of the WC (or typhoon) relative to the trough or the northwestern Pacific subtropical high under each synoptic weather pattern

	DTr	STH	Typh
Characteristics at 500 hPa	The deep trough to the north controls the central plain of East China	The northwestern Pacific subtropical high maintains around the south of the central plain of East China	A typhoon is located around the northwestern Pacific subtropical high, intensifying the transport of water vapor to the central plain of East China
Number and percentage of WC	44 (20.8%)	112 (52.8%)	56 (26.4%)
Number of proximal ERA-interim dates of WC	30	75	39
Location of WC (or typhoon) relative to the trough or subtropical high	WC is pre-trough (50%) or post-trough (50%)	WC is pre-trough (60%), or post-trough (20%), or in the flat westerly by the edge of the subtropical high (20%)	Typhoon is south to (70%), or west to (23%), or cut off (7%) the subtropical high

The STH pattern is featured with the northwestern Pacific subtropical high maintaining around the south of the central plain of East China, mostly interacting with a trough to the north. The convergence of westerly from the trough and southwest low-level jet from the northwest edge of the subtropical high apparently played an important role in the formation of the WC. This synoptic weather pattern was the most popular among the three patterns, accounting for 52.8% (112) of the total WC cases under study. Among all WC cases under this synoptic pattern, 60% were located pre-trough (e.g., Fig. 5a), 20% post-trough (e.g., Fig. 5b), and 20% in the flat westerly over the northern side of the northwestern Pacific subtropical high (e.g., Fig. 5c). Over the central plain of East China, moisture was abundant (precipitable water > 55 mm), mostly transported by low-level jets that were located near the northwest of the northwestern Pacific subtropical high (Fig. 5).

For the Typh pattern,the occurrence and development of the WC had some relation with typhoons over Southeast China or adjacent oceans, which probably intensified the transport of warm and moist air to the region. There are 56 WC cases over the central plain detected by TRMM under the Typh pattern, accounting for 26.4% of the total WC occurrences, which was comparable to that under the DTr pattern. The typhoons were located south to, west to, or cut across the northwestern Pacific subtropical high. The first category (e.g., Fig. 6a) was the most often (70%), the third was the least (7%), and the second in between (23%). Under the Typh weather pattern, air over the central plain of East China was warm and moist with large amount of precipitable water and high θ_e (Fig. 6), similar to the STH pattern.

4. Subseasonal variations of WC occurrences

The number of the WC occurrences over the central plain of East China during each half-month from 16 May to 31 August during 1998–2010 is shown in Fig. 7a. On the whole, a small fraction (8 cases; 4%) of the WC occurred in mid-to-end May (and early-to-mid June). The occurrence increased substantially in mid-to-end June (39 cases; 18%) probably owing to northward march of the East Asian summer monsoon, which is represented by the high-θ_e ($\geqslant 340$ K) air at 850 hPa (Ding and He, 2006) as shown in Fig. 1a. About half (101 cases; 48%) of the WC occurrences appeared in July with a peak during 1–15 July (53 cases), and 26% in August (56 cases), i.e., the WC in the central plain of East China occurred most often

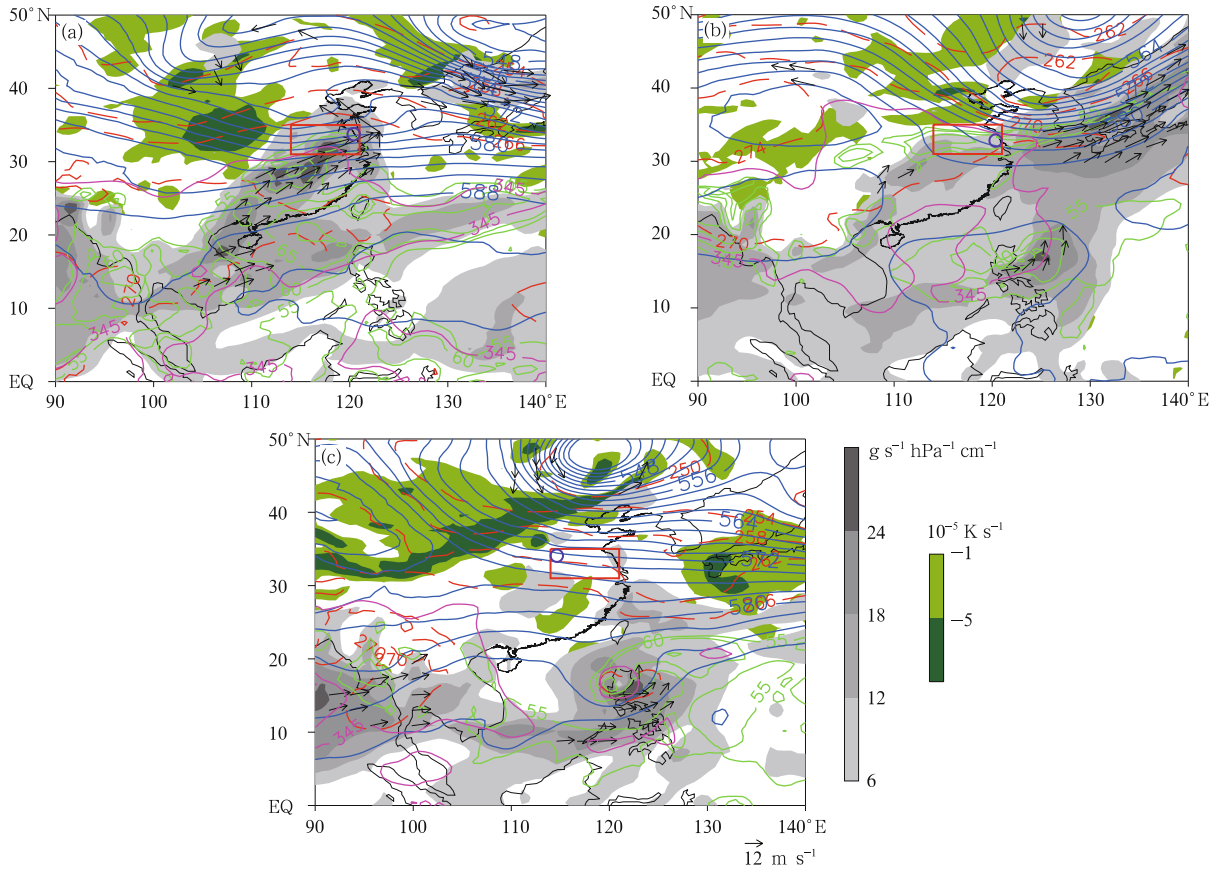

Fig. 4. Examples of environmental fields for the WC under the DTr pattern at (a) 0000 UTC 1 July 1998, (b) 1800 UTC 20 June 2005, and (c) 1200 UTC 17 May 2008. Plotted are geopotential height (blue line, with 20-geopotential meter intervals; 10 gpm), temperature (red dashed line, with 4-K intervals; K) and temperature advection (shadings in green) at 500 hPa, horizontal wind (arrow; only wind speed > 12 m s^{-1} are shown), θ_e of 345 K (purple contour) at 850 hPa, water vapor flux (gray shadings) at 925 hPa, and column-integrated precipitable water larger than 55 mm (green line, with 5-mm intervals). Locations of the WC and the central plain of East China are marked by the blue circle and the red rectangle, respectively.

from mid June to end of August with the peak in July. These results suggest that the WC in this region was mostly influenced by the summer monsoon, as the monsoonal air arrived at and moved over at least part of the region from mid June to end of August (Fig. 1a).

The WC occurrences under the three synoptic weather patterns exhibit distinctive subseasonal variations (Fig. 7b). The WC cases of the DTr pattern emerged the earliest (8 cases during 16–31 May, 18% of this pattern) among the three weather patterns, and they occurred the most often in the second half of June (16 cases, about 36% of this pattern). For this type of WC during mid May to July, the subtropical high ridge line was located at 25°N or further to the south (Figs. 8a, 8d, 8g, and 8j), indicating that the monsoonal flows could not significantly impact the central plain of East China; on the other hand, the deep trough in the north always dominated this region. Moreover, for the DTr type WC, the western edge point of the subtropical high was mostly located east of 110°E (Figs. 8a, 8d, 8g, and 8j), suggesting eastward retreat of the subtropical high accompanying southward extension of the deep trough.

Subseasonal variations of the WC occurrence under the STH pattern (Fig. 7b) present a major peak

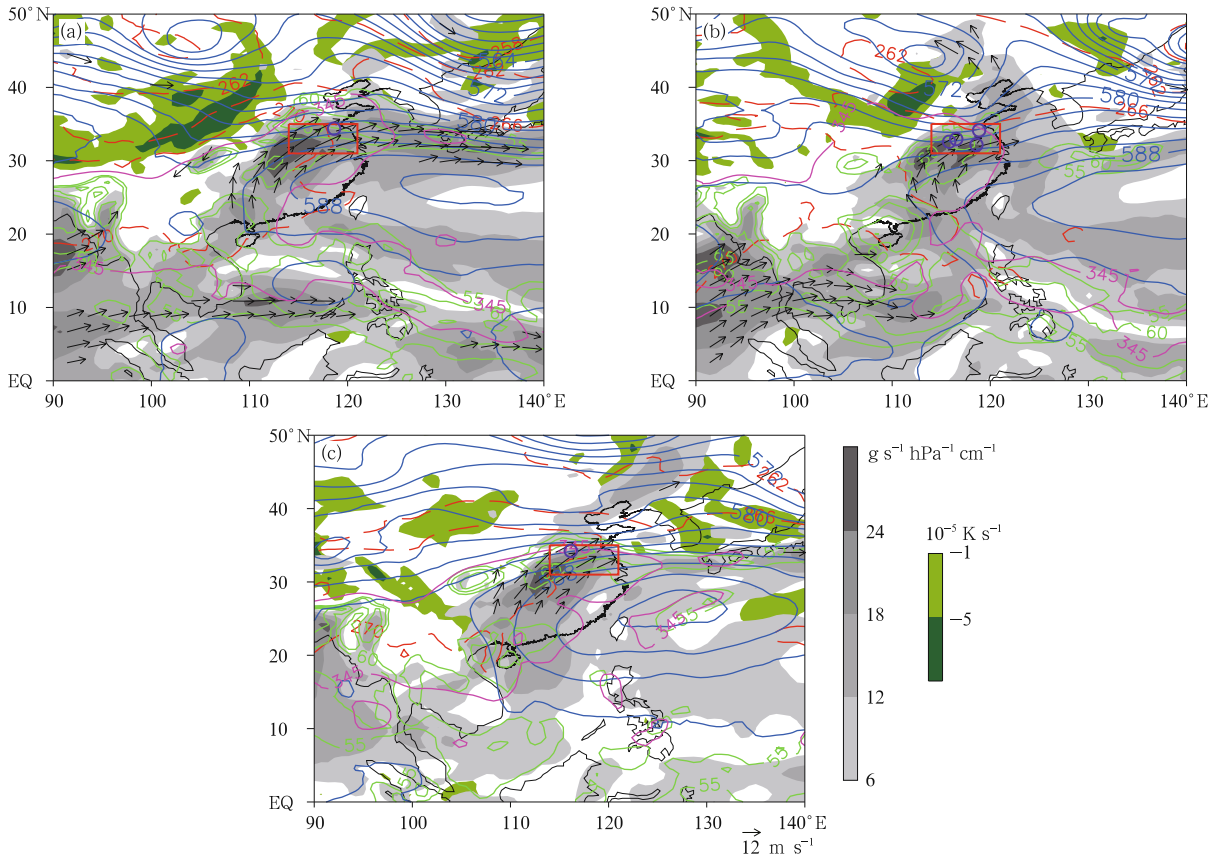

Fig. 5. As in Fig. 4, but for the WC under the STH pattern at (a) 1800 UTC 28 June 2001, (b) 0000 UTC 29 June 2006, and (c) 0000 UTC 12 July 2003, representing the situations of WC being located pre-trough, post-trough, and in flat westerly, respectively.

in the first half of July (35 cases) and a third peak in the second half of June (21 cases). The two peaks together contributed 50% to the total WC occurrences under the STH pattern, i.e., mid June to mid July was the main period of the WC occurrence under this pattern. This period corresponds to the Meiyu period of East China (Luo et al., 2013), when the northern edge of the southwesterly low-level jet was located over the central plain of East China (Fig. 1a). During this period, the ridge line of the northwestern Pacific subtropical high over 110°–130°E was located over 25°–30°N and the western ridge point of the subtropical high was mostly around or to the east of 110°E (Figs. 8e and 8h), favoring transport of moisture to the region along the western and northwestern sides of the subtropical high (Fig. 5). For the STH-type WC cases in mid July to August, the western ridge points of the subtropical high were mostly located more westward (Figs. 8k and 8n) than in mid June to mid July under the STH pattern (Figs. 8e and 8h) and also than the other two patterns in mid July to August (Figs. 8j, 8l, 8m, and 8o). Its location to the west of 110°E indicates that the subtropical high was strong enough to control all of Southeast China including the central plain of East China. Under this condition in mid July to August, transport of water vapor to the central plain of East China was generally weaker than that during mid June to mid July under the STH pattern.

Most WC cases under the Typh pattern occurred in July and August (Fig. 7b), as the typhoons influencing rainfall over China usually occurred from July (Ren et al., 2002), with 23 cases (41% of this pattern) in July and 28 cases (50% of this pattern) in August. Only 3 WC cases (9%) under this pattern occurred

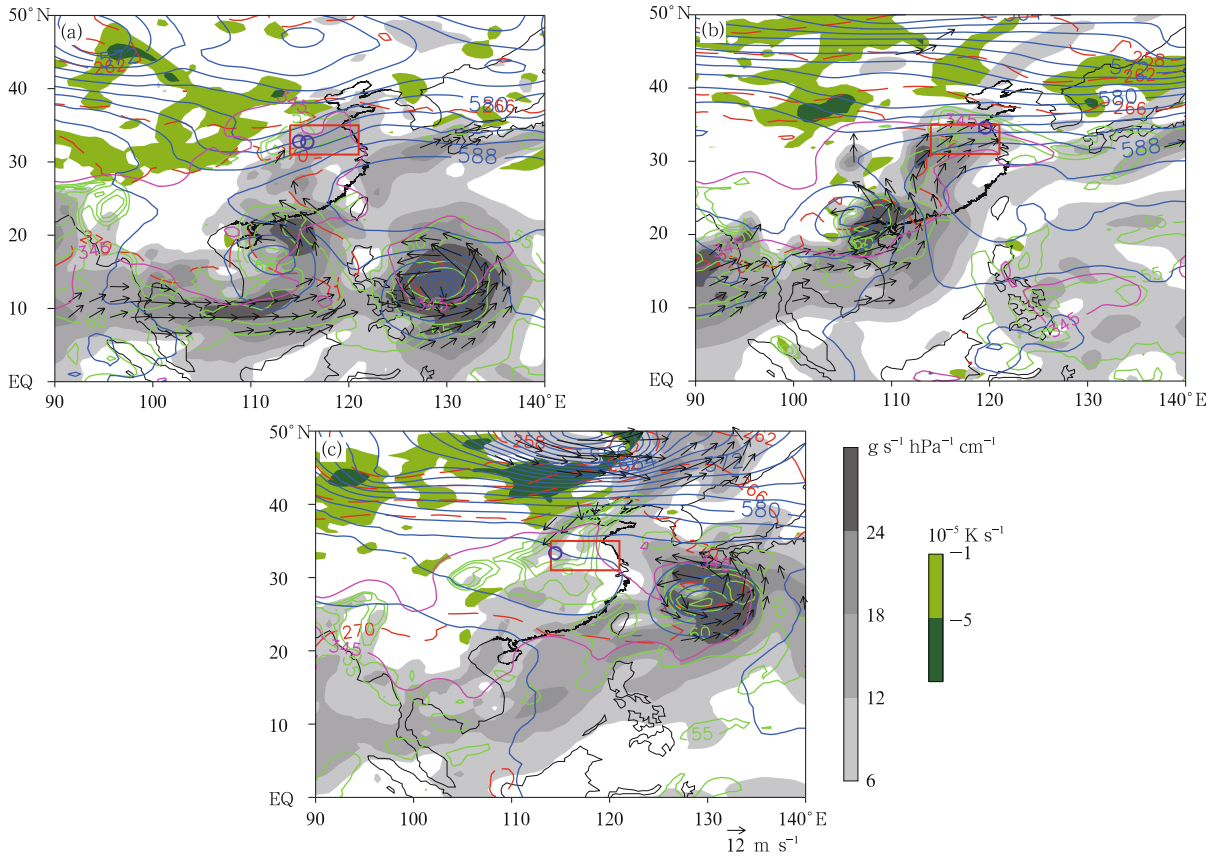

Fig. 6. As in Fig. 4, but for the WC under the Typh pattern at (a) 1800 UTC 20 July 2003, (b) 0000 UTC 26 August 2003, and (c) 0000 UTC 28 July 2000, representing the situations of typhoon being located south to, west to, and across off the subtropical high, respectively.

before July. All of the 3 cases belong to the situation of typhoon across off the subtropical high. For some cases under the Typh pattern in mid July to August, the subtropical high ridge line tended to locate to the north of 35°N (Figs. 8l and 8o), suggesting that the WCs could form over the central plain of East China under the effect of typhoon when the subtropical high ridge line was located to the north of the region.

5. Occurrences of severe convective weather

Whether the WC is accompanied with severe convective weather is worth studying, as severe convective weather can cause serious disaster to humanity. Table 3 gives the statistics of severe convective weather events, including thunderstorm, gale, hail, and short-duration heavy rainfall, in the central plain of East China when the WC occurrences were detected by TRMM in the region. Comparisons of occurrences of the four kinds of severe convective weather events under the three synoptic weather patterns are described below in the order of their occurrences from the most to the least.

Table 3 reveals the following facts:

1) Thunderstorms occurred during nearly all dates (93%–97%) of the WC under the DTr, STH, and Typh patterns, suggesting that the WC cases were always associated with thunderstorms even for different synoptic weather situations.

2) A majority (69%–85%) of the WC cases in the central plain of East China occurred with short-duration heavy rainfall ($R_{6h} \geqslant 20$ mm) over the region. The percentages decreased to 52%–64% for $R_{6h} \geqslant 30$ mm and further to 38%–42% $R_{6h} \geqslant 50$ mm. Among

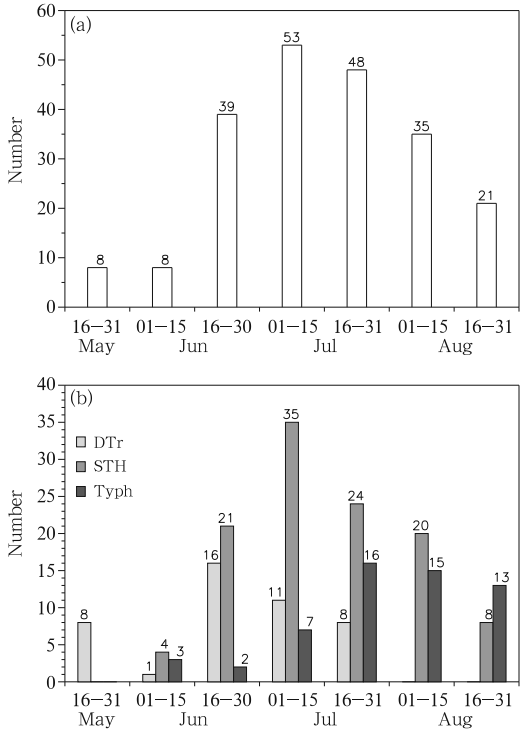

Fig. 7. Numbers of the WC cases in the central plain of East China during each half-month period from 16 May to 31 August during 1998–2010: (a) all WC cases and (b) the WC cases under DTr, STH, and Typh synoptic patterns.

the three synoptic patterns, the short-duration heavy rainfalls occurred the least often under the DTr pattern. The occurrence frequencies of the short-duration heavy rainfalls with $R_{6h} \geqslant 20$ mm were the largest under the Typh pattern (85%); that with $R_{6h} \geqslant 30$ mm and $R_{6h} \geqslant 50$ mm was the largest under the STH pattern (65% and 42%, respectively); they were all the least under the DTr pattern.

3) About a quarter of the WC cases occurred with gale (i.e., surface wind speed > 17 m s^{-1}). Gale occurred the most often (28%) for the WC under the DTr pattern, the least (21%) under the STH pattern, and in between (23%) under the Typh.

4) Under the three synoptic weather patterns of the WC, hail occurred very rarely, with only 0% (DTr), 1.4% (STH), and 2.6% (Typh) of the cases.

6. Relation of environmental atmospheric conditions to the convective weather

This section gives detailed quantitative comparisons of environmental atmospheric thermodynamic conditions of the WC cases among the three synoptic weather patterns (Figs. 9–12), hoping to better understand the similarities and differences in the occurrences of severe convective weather in association with the WC over the central plain of East China under the three synoptic patterns. Differences and similarities in the thermodynamic conditions among the three synoptic patterns are discussed below in the context of their possible relation to the various convective weather phenomena.

6.1 Conditions related to thunderstorm occurrence

Development of thunderstorms always needs large instable energy and abundant moisture (Doswell, 1987; Johns and Doswell, 1992). The cumulative distributions of vertical profile of convective available potential energy (CAPE) in the central plain of East China during the dates when the WC occurrences were detected over the region by TRMM show that the largest CAPE existed for the air parcel being lifted

Table 3. Numbers of WC times with valid surface observation, and numbers and fractions (%) of severe weather phenomena when the WC occurrences were detected by TRMM in the central plain of East China under the DTr, STH, and Typh patterns, respectively

		DTr	STH	Typh
Valid WC times		29	72	39
Thunderstorm		27 (93%)	70 (97%)	38 (97%)
Gale		8 (28%)	15 (21%)	9 (23%)
Hail		0 (0%)	1 (1.4%)	1 (2.6%)
Short-duration heavy rainfall:	$R_{6h} \geqslant 20$ mm	20 (69%)	59 (82%)	33 (85%)
	$R_{6h} \geqslant 30$ mm	15 (52%)	47 (65%)	25 (64%)
	$R_{6h} \geqslant 50$ mm	11 (38%)	30 (42%)	16 (41%)

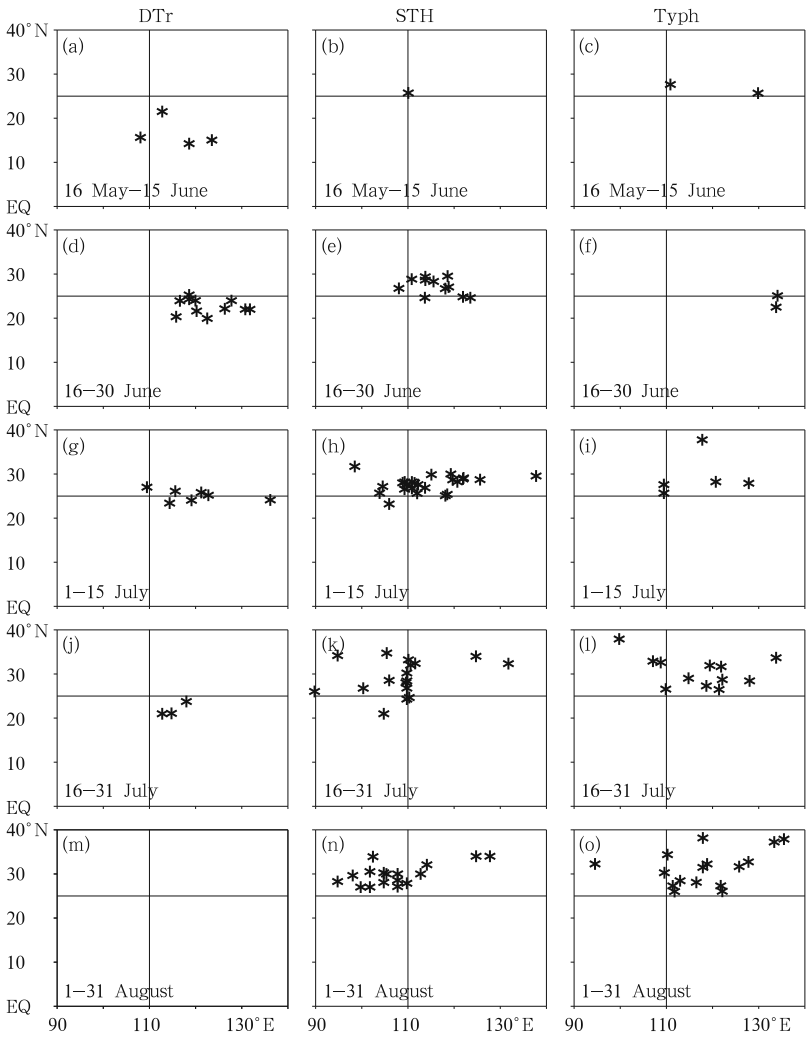

Fig. 8. Joint scatter distributions of the latitude of ridge line over 110°–130°E and the longitude of western ridge point of the northwestern Pacific subtropical high during the dates when the WC occurred under the DTr, STH, and Typh patterns, respectively, during (a–c) 16 May–15 June, (d–f) 16–30 June, (g–i) 1–15 July, (j–l) 16–31 July, and (m–o) 1–31 August of 1998–2010.

from the surface, i.e., the most unstable air was near the surface for all the synoptic patterns (Fig. 9a). The median values of CAPE at the surface were about 1000 J kg^{-1}, i.e., nearly half of the CAPE values were larger than 1000 J kg^{-1}, satisfying the instability condition for the development of convective storms proposed by Weisman and Klemp (1982). Meanwhile, the median values of precipitable water under DTr, STH, and Typh were 50.4, 59.9, and 59.3 mm (Fig. 10a), respectively, comparable to the averaged precipitable water (56 mm) in the environment of squall lines in East China (Meng et al., 2013), reflecting abundant moisture supply for the formation of the WC. Therefore, the large instability energy and plentiful moisture in the WC's environment under all synoptic patterns formed favorable conditions for convection development, supporting the conclusion that the WC cases were always companied with thunderstorms (Section 5).

6.2 Conditions related to short-duration heavy rainfall

The generally abundant moisture (Fig. 10a), combined with large CAPE (Fig. 9a), over the central

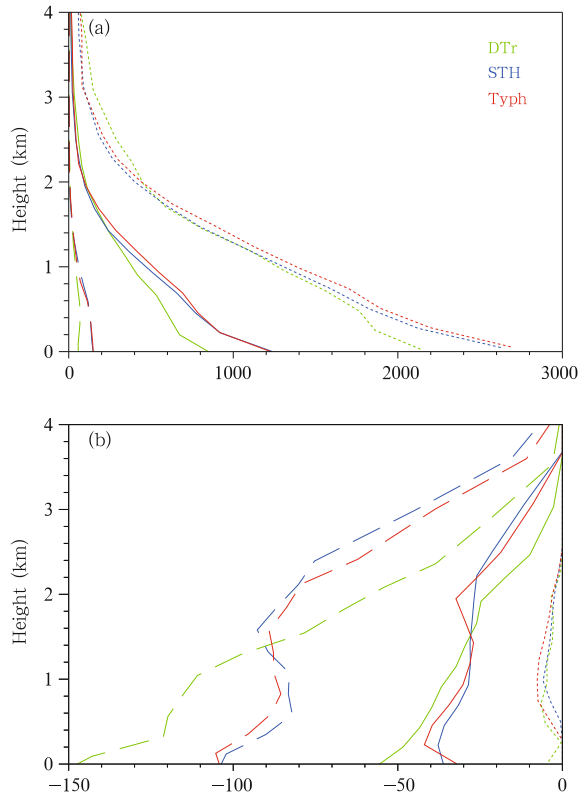

Fig. 9. Vertical profiles of (a) CAPE and (b) CIN derived from parcel ascents from different vertical levels in the central plain of East China during the days when the WC was detected by TRMM under the DTr (green), STH (blue), and Typh (red) patterns, respectively. The dashed, solid, and dotted lines represent the 10th, 50th, and 90th percentile, respectively. The results are based on the ERA-interim data.

plain of East China for the WC under study was probably the most important reason for the relatively frequent occurrence of short-duration heavy rainfall under the three synoptic patterns (Table 3). This is consistent with the result of Zheng (2013): the short-duration heavy rainfall over central East China tends to be associated with moist environment, i.e., the precipitable water greater than 50 mm.

However, differences in the vertical distributions of air temperature and moisture among the three synoptic patterns are noticeable (Figs. 10b and 11), which probably contribute to the previously discussed difference in the occurrence of short-duration heavy rainfall. The averaged air temperature and dew point temperature at each level of the troposphere (1000–200 hPa) under the DTr pattern were lower than those under the STH and Typh patterns (Fig. 11a), suggesting that there existed driest and coldest air over the central plain of East China under the DTr pattern. The averaged profiles of air temperature and dew point temperature differed little between the STH and Typh patterns, reflecting their similar temperature and humidity conditions. Comparisons of cumulative distributions of precipitable water and θ_e among the three

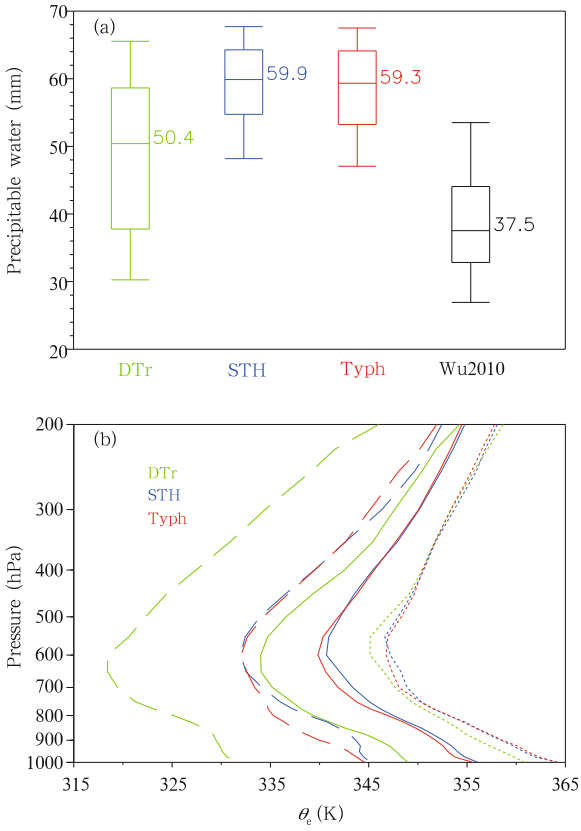

Fig. 10. (a) Box-and-whisker plots of precipitable water (mm) in the central plain of East China when the WC was detected by TRMM over the region under the DTr, STH, and Typh synoptic weather patterns, as well as for the 39 hail events provided by Wu (2010), showing the median (short line in the box), interquartile range (rectangle), and outliers (i.e., the 10th and 90th percentile as whiskers) with the median values labeled on the right. (b) Vertical profile of θ_e in the central plain of East China under the three synoptic weather patterns: DTr (green), STH (blue), and Typh (red), with the dashed, solid, and dotted lines representing the 10th, 50th, and 90th percentile, respectively. The results are based on the ERA-interim data.

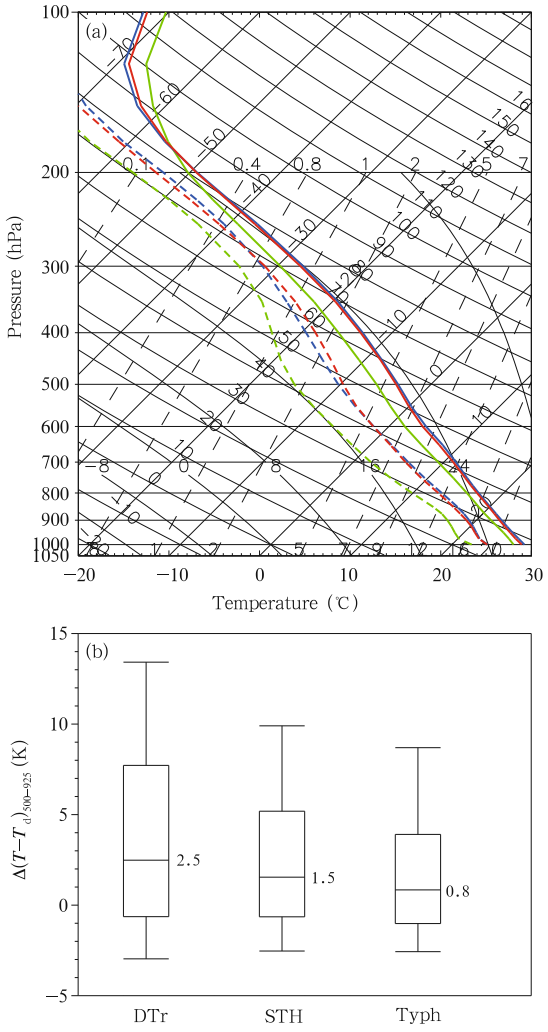

Fig. 11. (a) Vertical profiles plotted on the skew T-log$p$ diagram of the composite temperature (thick solid color lines) and dew point temperature (thick dashed color lines) in the central plain of East China during the days when the WC was detected by TRMM under the synoptic weather patterns of DTr (green lines), STH (blue lines), and Typh (red lines) during 1998–2010. (b) Box-and-whisker plots of the difference in dew-point depression between 500 and 925 hPa over the central plain of East China under the three synoptic weather patterns of the WC, showing the median (short line in the box), interquartile range (rectangle), and outliers (i.e., the 10th and 90th percentile as whiskers) with the median values labeled on the right. The results are based on the ERA-interim data.

weather patterns (Fig. 10) further confirm the driest and coldest air under the DTr pattern: the median values of precipitable water under the DTr pattern was 50.4 mm, substantially smaller than the STH (59.9 mm) and Typh (59.3 mm) patterns (Fig. 10a); the 10th, 50th, and 90th percentiles of the profiles of θ_e under the DTr pattern were all lower than those under the other two patterns (Fig. 10b), probably due to stronger transport of warm and moist air into the central plain of East China by the low-level flows in association with the subtropical high and typhoons under the latter two patterns. In addition, the largest precipitable water (59.9 mm) and the highest values of θ_e in the central plain of East China were both found under the STH pattern, suggesting the highest moisture under this pattern. Therefore, the driest and coldest air over the central plain of East China under the DTr pattern induced the least occurrences of short-duration heavy rainfall under this pattern (Table 3), while the most abundant moisture under the STH pattern supported the most occurrences of short-duration heavy rainfall ($R_{6h} \geqslant 30$ mm and $R_{6h} \geqslant 50$ mm; see Table 3).

6.3 Conditions related to gale formation

Occurrence of gale is also related to vertical distribution of air humidity (e.g., Zheng, 2013). The maximum values of depression of dew point ($T - T_d$) under the three synoptic weather patterns were all in the mid troposphere with the largest under the DTr pattern (Fig. 11a), likely reflecting the largest impacts of dry air invasion in the mid troposphere in this case. For example, the depression of dew point at 500 hPa under the DTr pattern is 9.1 K, which was 2.5 and 3.4 K larger than those under the STH and Typh pattern, respectively. Moreover, the DTr pattern had larger differences in depression of dew-point between mid and low levels (Fig. 11b), indicating larger differences of air humidity between the low and mid troposphere under the DTr pattern than under the other two patterns. These features of vertical distribution of air humidity under the DTr pattern were more favorable for gale formation, because when the drier air in the mid troposphere falling down encounters moister air at the low level, evaporation of the moist air and the resultant latent cooling will increase, and thus the downdraft will strengthen. This is consistent with the

larger occurrences (28%) of gale in association with the WC under the DTr pattern than under the STH (21%) and Typh (23%) pattern. On the other hand, although the Typh pattern was associated with the least moisture difference between mid and low levels (Fig. 11b), the occurrence of gale was not the least under the Typh pattern, due likely to the acceleration of wind by the effect of typhoon.

6.4 Conditions related to hail occurrence

Three important environmental conditions for presence of hail at the surface are concluded in previous studies (Das, 1962; John and Doswell, 1992; Groenemeijer and Delden, 2007): (1) large thermal buoyancy (represented by CAPE), (2) strong vertical wind shear, and (3) moderate freezing level ($H_{\rm fz}$). These have been applied to studies of dynamic and thermodynamic environment for hail in, e.g., northern Greece (Sioutas and Flocas, 2003) and China (Xie et al., 2008). To obtain quantitative environmental conditions favoring occurrence of hail in central plain of East China, we derived the statistics of three parameters (CAPE, vertical wind shear between 500 hPa and near surface, and $H_{\rm fz}$) 0–12 h before 39 hail events (Wu, 2010; herein Wu2010) that occurred in the land region of 30°–40°N and east of 110°E during May–August of 2002–2009 based on sounding data. It is found that 85% of these hail-producing storms occurred when the three conditions were satisfied simultaneously: 1) CAPE $\geqslant$ 1000 J kg^{-1}, 2) vertical wind shear $V_{\rm shr} \geqslant 1\times10^{-3}$ s^{-1}, and 3) $H_{\rm fz} \leqslant$ 5.0 km. The three parameters were also calculated for the WC cases under study, by using the 6-h ERA-interim data 3–9 h before the WC occurrence detected by TRMM. Figures 12a–c show the joint distributions of $H_{\rm fz}$ and $V_{\rm shr}$ under the condition of CAPE $\geqslant$ 1000 J kg^{-1}. It is found that $H_{\rm fz}$ was mostly above 5 km under the STH pattern (Fig. 12b), which was probably one of the major reasons for the lack of hail presence at the surface under the STH pattern. However, for the DTr, STH, and Typh pattern, respectively, 55%, 12%, and 19% of the samples satisfied the above three favorable environmental conditions (Figs. 12a–c), but without hail on the ground.

To further explore possible reasons for the lack of hail in these WC samples, averaged profiles of temperature and dew point of these cases were compared to those of the 39 hail events in Wu2010 (Figs. 12d–f). This analysis was conducted because hail in China is speculated to be sensitive to air humidity based on the spatial and seasonal distributions of hail in China (i.e., hail is rare in very wet areas and relatively rare during rainy seasons; Zhang et al., 2008). The results show that the entire troposphere was much moister for the WC under the three synoptic patterns (Figs. 12d–f) than that of the 39 hail events of Wu2010. This is consistent with the substantially larger precipitable water for the WC cases (median values of 50.4–59.9 mm) than for the 39 hail events (37.5 mm) (Fig. 10a). Therefore, the environmental air seemed to be too humid to form hail when the WC was present over the central plain of East China.

7. Concluding remarks

In this study, wide convection (WC) is defined as contiguous convective echoes over 40 dBZ with nonzero near surface rainfall rate from the TRMM PR (Iguchi et al., 2000) over a horizontal area exceeding 1000 km^2. The flat land region over the central East China (31°–35°N, 114°–121°E; referred to as central plain of East China for simplicity) sees the maximum frequency of WC occurrence from the onset of the SCS summer monsoon to the end of August during 1998–2010. For the WC occurrences over this region, three representative synoptic weather patterns are identified, and occurrences of severe convective weather phenomena in association with the WC are then examined, followed by quantifying the corresponding atmospheric thermodynamic conditions. The major conclusions are as follows.

(1) Based on the atmospheric circulation at 500 hPa when the WC was present in the central plain of East China, the environmental fields of WC are classified into three weather patterns by using an objective classification method: deep-trough-in-the-north (DTr), subtropical-high-maintenance (STH), and typhoon-effect (Typh), accounting for 20.8%, 52.8%, and 26.4%, respectively, of the total WC occurrences. Among the three patterns, the WC under

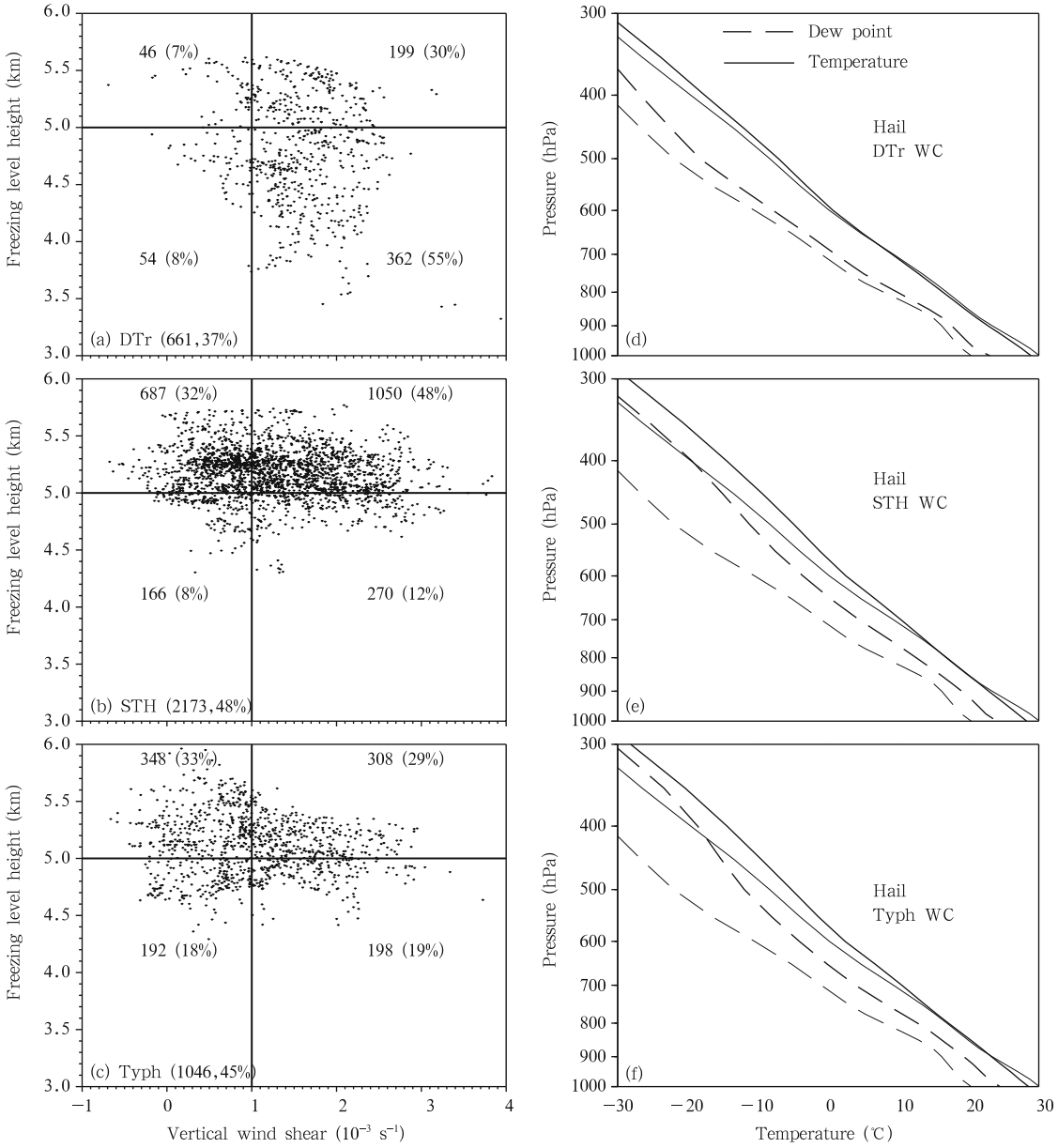

Fig. 12. (a–c) Joint scatter distributions of freezing level height ($H_{\rm fz}$; km) and vertical wind shear between 500 hPa and 10 m above the ground ($V_{\rm shr}$; 10^{-3} s^{-1}) in the condition of CAPE $\geqslant$ 1000 J kg^{-1} over the central plain of East China under three synoptic weather patterns: (a) DTr, (b) STH, and (c) Typh. The numbers and percentages at the bottom of the panels are the total numbers and fractions of grid points in the central plain of East China with CAPE $\geqslant$ 1000 J kg^{-1} under the corresponding synoptic weather pattern. The four pairs of number and percentage in each of the panels represent the number and fraction of grid points located in the four portions of the $V_{\rm shr}$–$H_{\rm fz}$ plane. (d–f) Averaged profiles of temperature (solid lines) and dew point (dashed lines) representing the environmental conditions of storms. The lines in gray represent those for the 39 hail-producing storms collected by Wu2010, while the lines in black are averaged over grid points in the central plain of East China with CAPE $\geqslant$ 1000 J kg^{-1}, $H_{\rm fz} \leqslant$ 5 km, and $V_{\rm shr} \geqslant$ 1×10^{-3} s^{-1} for the WC under the (d) DTr, (e) STH, and (f) Typh synoptic pattern. The results are based on the ERA-interim data 0–6 h before the WC occurrence detected by TRMM in the region.

the DTr pattern started to emerge the earliest (16–31 May) and occurred the most often in the second half of June; the WC under the STH pattern had a significant peak in the first half of July; those under the Typh pattern mainly occurred in July and August. On the whole, the WC in the central plain of East China mostly formed under the influence of the Asian summer monsoon during 16 June–31 August, with a main peak of occurrence in July.

(2) The WC occurrences in the central plain of East China were mostly companied with thunderstorms, i.e., for 93%, 97%, and 97% of the times under the DTr, STH, and Typh pattern. But WC occurred very rarely (< 3%) with hail on the ground. Under the various weather patterns, a majority (69%–85%) of the WC cases occurred with short-duration heavy rainfall ($R_{6h} \geqslant 20$ mm), with the DTr pattern seeing the smallest occurrence. Gales occurred the most often (28%) under the DTr pattern and the least (21%) under the STH pattern.

(3) The large CAPE and abundant moisture in the environment of the WC made thunderstorms always accompany. Among the three weather patterns, the DTr pattern featured the least occurrences of short-duration heavy rainfall, the lowest rainfall amount, and the smallest rainy coverage, probably due to the driest and coldest air in the region under this weather pattern; the STH pattern saw the most occurrences of short-time heavy rainfall ($R_{6h} \geqslant 30$ mm and $R_{6h} \geqslant 50$ mm) over the region, supported by the most abundant moisture and warmest air. Gales occurred more often under the DTr pattern than the other two patterns, probably contributed by the stronger dry air invading in the mid troposphere and the larger difference in depression of dew-point between mid and low troposphere under the DTr pattern. The rare occurrences of hail during the WC cases were possibly owing to the humid environmental air over the region under the various weather patterns. Under the STH pattern, lack of hail on the ground could also be contributed by the high freezing levels (mostly above 5 km), which made it hard for hailstones, if any, formed aloft in the storms, to survive on their way falling toward the ground.

This study provides some statistical characteristics of synoptic patterns, surface weather phenomenon, and thermodynamic conditions for the WC occurrences in the flat land region of central East China. Mechanisms that govern the occurrence and development of the WC, as well as the relation between the environmental conditions and severe weather phenomena are not very clear yet. These will be further explored in future studies using high-resolution observations and numerical simulations.

Acknowledgments. We acknowledge the National Meteorological Information Center of China Meteorological Administration for providing the gridded hourly precipitation data and surface meteorological observations, and University of Utah for providing the TRMM data. Many thanks go to Dr. Tao LUO for downloading the ERA-interim data from the Research Data Archive maintained by the Computational and Information Systems Laboratory at NCAR, USA. Finally, we thank the anonymous reviewers for helpful comments.

REFERENCES

Anderberg, M. R., 1973: *Cluster Analysis for Applications*. Academic Press, New York, 359 pp.

Awaka, J., T. Iguchi, and K. Okamoto, 1998: Early results on rain type classification by the Tropical Rainfall Measuring Mission (TRMM) precipitation radar. Proc. 8th URSI Commision F Triennial Open Symposium on Wave Propagation and Remote Sensing, Aveiro, Portugal, September 22–25, Universidade de Aveiro, 143–146.

Cecil, D. J., E. J. Zipser, and S. W. Nesbitt, 2002: Reflectivity, ice scattering, and lightning characteristics of hurricane eyewalls and rainbands. Part I: Quantitative description. *Mon. Wea. Rev.*, **130**, 769–784.

Cecil, D. J., S. J. Goodman, D. J. Boccippio, et al., 2005: Three years of TRMM precipitation features. Part I: Radar, radiometric, and lightning characteristics. *Mon. Wea. Rev.*, **133**, 543–566.

Das, P., 1962: Influence of wind shear on the growth of hail. *J. Atmos. Sci.*, **19**, 407–414.

Dee, D. P., S. M. Uppala, A. J. Simmons, et al., 2011: The ERA-interim reanalysis: Configuration and performance of the data assimilation system. *Quart. J.*

Roy. Meteor. Soc., **137**, 553–597.

Ding, Y. H., 1994: *Monsoons over China*. Kluwer Academic, 419 pp.

Ding, Y. H., and J. C. L. Chan, 2005: The East Asian summer monsoon: An overview. *Meteor. Atmos. Phys.*, **89**, 117–142.

Ding Yihui and He Chun, 2006: The summer monsoon onset over the tropical eastern Indian Ocean: The earliest onset process of the Asian summer monsoon. *Adv. Atmos. Sci.*, **23**, 940–950.

Ding, Y. H., and Z. Wang, 2008: A study of rainy seasons in China. *Meteor. Atmos. Phys.*, **100**, 121–138.

Doswell, C., 1987: The distinction between large-scale and mesoscale contribution to severe convection: A case study example. *Wea. Forecasting*, **2**, 3–16.

Groenemeijer, P., and A. Delden, 2007: Sounding-derived parameters associated with large hail and tornadoes in the Netherlands. *Atmos. Res.*, **83**, 473–487.

Houze, R. A. Jr., D. C. Wilton, and B. F. Smull, 2007: Monsoon convection in the Himalayan region as seen by the TRMM precipitation radar. *Quart. J. Roy. Meteor. Soc.*, **133**, 1389–1411.

Huang, R., G. Huang, and Z. Wei, 2004: Climate variations of the summer monsoon over China. *East Asian Monsoon*. C. P. Chang, Ed, World Scientific, 213 pp.

Iguchi, T., T. Kozu, R. Meneghini, et al., 2000: Rain-profiling algorithm for the TRMM precipitation radar. *J. Appl. Meteor.*, **39**, 2038–2052.

Johns, R., and C. Doswell, 1992: Severe local storms forecasting. *Wea. Forecasting*, **7**, 588–612.

Kawanishi, T., H. Kuroiwa, M. Kojima, et al., 2000: TRMM precipitation radar. *Adv. Space Res.*, **25**, 969–972.

Kummerow, C., Y. Hong, W. S. Olson, et al., 2001: The evolution of the Goddard profiling algorithm (GPROF) for rainfall estimation from passive microwave sensors. *J. Appl. Meteor.*, **40**, 1801–1820.

Liu, C., 2007: University of Utah TRMM precipitation and cloud feature database: Description version 1.0. University of Utah, 22 pp. [Available online at http://trmm.chpc.utah.edu/docs/trmm_database_description_v1.0.pdf.]

Liu, C., E. Zipser, D. J. Cecil, et al., 2008: A cloud and precipitation feature database from 9 years of TRMM observations. *J. Appl. Meteor. Climatol.*, **47**, 2712–2728.

Luo, Y., H. Wang, R. Zhang, et al., 2013: Comparison of rainfall characteristics and convective properties of monsoon precipitation systems over South China and the Yangtze and Huai River basin. *J. Climate*, **26**, 110–132.

Meng, Z., D. Yan, and Y. Zhang, 2013: General features of squall lines in East China. *Mon. Wea. Rev.*, **141**, 1629–1647.

Ren Fumin, G. Byron, and E. David, 2002: Typhoon impacts on China's precipitation during 1957–1996. *Adv. Atmos. Sci.*, **19**, 943–952.

Romatschke, U., S. Medina, and R. A. Houze, 2010: Regional, seasonal, and diurnal variations of extreme convection in the South Asian Region. *J. Climate*, **23**, 419–439.

Simmons, A. J., S. M. Uppala, D. Dee, et al., 2007: ERA-Interim: New ECMWF Reanalysis Products from 1989 Onwards. Newsletter 110–Winter 2006/07, ECMWF, 11 pp.

Sioutas, M., and H. Flocas, 2003: Hailstorms in northern Greece: Synoptic patterns and thermodynamic environment. *Theor. Appl. Climatol.*, **75**, 189–202.

Wang, B., Lin Ho, Y. S. Zhang, et al., 2004: Definition of the South China Sea monsoon onset and commencement of the East Asian summer monsoon. *J. Climate*, **17**, 699–710.

Weisman, M. L., and J. B. Klemp, 1982: The dependence of numerically simulated convective storms on vertical wind shear and buoyancy. *Mon. Wea. Rev.*, **110**, 504–520.

Wu Jiankun, 2010: Preliminary analysis of environmental conditions and radar echo features of hail in China. Master dissertation, Chinese Academy of Meteorological Sciences, Beijing, 105 pp. (in Chinese)

Xie, B. G., Q. H. Zhang, and Y. Q. Wang, 2008: Trends in hail in China during 1960–2005. *Geophys. Res. Lett.*, **35**, L13801, doi: 10.1029/2008GL0304067.

Zhang, C., Q. Zhang, and Y. Wang, 2008: Climatology of hail in China: 1961–2005. *J. Appl. Meteor.*, **47**, 795–804.

Zheng Linlin, 2013: The characteristics of mesoscale convective systems over Yellow River and Huai River basins. Ph. D. dissertation, Institute of Atmospheric Physics, Chinese Academy of Sciences, 152 pp. (in Chinese)

Zheng, L., J. Sun, X. Zhang, et al., 2013: Organizational modes of mesoscale convective systems over central East China. *Wea. Forecasting*, **28**, 1081–1098.

Zipser, E., D. J. Cecil, C. Liu, et al., 2006: Where are the most intense thunderstorms on earth. *Bull. Amer. Meteor. Soc.*, **87**, 1057–1071.